Available online at www.sciencedirect.com

ScienceDirect

IFAC PapersOnLine 53-1 (2020) 422–427

IFAC Papers Online CONFERENCE PAPER ARCHIVE

Wheel Slip Regulation Of Electrified Heavy Road Vehicles Using Regenerative Braking

Kesavan Valis Subramaniyam, Shankar C. Subramanian *

* *Department of Engineering Design, IIT Madras, Chennai 600036, India (Tel: +91-44-22574705; e-mail: shankarram@iitm.ac.in).*

Abstract: This paper proposes a control scheme to use regenerative braking for Wheel Slip Regulation (WSR) in Heavy Commercial Road Vehicles (HCRVs). Typically, in HCRVs, WSR is achieved using pneumatic friction brakes. However, in electrified vehicles regenerative braking is available and this can be beneficial as electrical machines have higher bandwidth compared to a pneumatic brake system. In this study, a sliding mode control based active co-operative braking strategy is proposed for WSR in an electrified HCRV. The proposed control strategy was programmed in MATLAB/Simulink® and implemented in a Hardware-in-loop brake system. The experimental results showed that the proposed active co-operative braking strategy reduced the Mean Absolute Percentage Error in tracking slip ratio in the range of 6.7 % to 1.1 % compared to conventional friction braking for different operating conditions. This reduced the stopping distance in the range of 3.5 % to 0.6 %. Thus, co-operative braking provided better slip tracking leading to reduced stopping distance.

Keywords: electric vehicles, hybrid electric vehicles, heavy commercial road vehicles, sliding mode control, regenerative braking, wheel slip regulation.

1. INTRODUCTION

Generally, vehicles are controlled by the driver using accelerator pedal, braking pedal and steering wheel. However, in an emergency situation such as on slippery road surfaces and critical road maneuvers, a driver cannot react very quickly and the drivers command may not be sufficient to control the vehicle. These situations may cause vehicle instability and thereby accidents. The World Health Organization estimated that road traffic injuries are currently the eighth leading cause of death globally in the year of 2016, and predicted that are nearly 3700 fatalities on the world's roads every day [World Health Organization (2018)]. International Road Federation organization reported that India is the most affected country in the world in the year 2016, accounting for 10 % of global accidents. In India, amongst the road vehicle categories, Heavy Road Commercial Vehicles (HCRVs) contributed the second-highest share in total road accident fatalities accounting for 32.6 % of total fatalities in the year 2017 [Ministry of Road Transport & Highways, Transport Research Wing (New Delhi, India, 2017.)].

Active safety systems can be used to prevent road accidents and associated fatalities. These systems use wheel slip ratio (λ), yaw rate (r)), drivers command such as braking torque, steering angle and the environment (tire-road friction coefficient(μ), and lane width (L_w)) as inputs and accordingly take the necessary action to make the vehicle stable, as represented in Fig. 1. Here, $T_{b,a}$ and $T_{b,d}$ indicate actual and desired braking torque respectively, δ_a and δ_d indicate actual and desired steering input respectively. Typically, the vehicle's brake system is designed by considering a fully laden vehicle and dry road operating condition. For other operating conditions such as partially

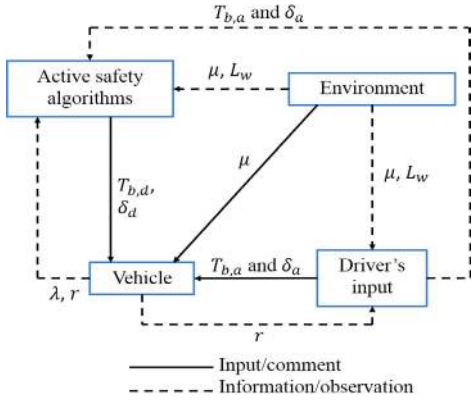

Fig. 1. Vehicle's active safety system layout

unladen on a dry road, fully unladen on dry, wet and snowy roads, the demanded brake force corresponding to full brake pedal displacement may exceed the maximum braking force limit that can be sustained at a tire-road interface. This causes wheel lock during emergency braking. Wheel locking during braking causes loss of steering control and vehicle spin out.

To avoid wheel lock during such scenarios, an Anti-lock Brake System (ABS) is used in a vehicle. Data from National Highway Traffic Safety Administration (NHTSA), Department of Transportation, U.S. government indicates that ABS reduced vehicle crashes by 13 % for HCRVs in the year 2010 [Allen (2010)]. One of the critical variable used in regulation of wheel slip is the wheel slip ratio which is defined as

$$\lambda(t) = \frac{u(t) - \omega(t)R_t}{u(t)}, \tag{1}$$

10.1016/j.ifacol.2020.06.071

where u is the longitudinal vehicle speed, R_t is the tire radius and ω is the wheel angular speed. To utilize the maximum braking force that can be generated by the tire, it is necessary to maintain the slip ratio in the desired region as shown in Fig. 2. The desired slip ratio can be achieved by controlling the braking torque or pressure during braking application. In literature, different

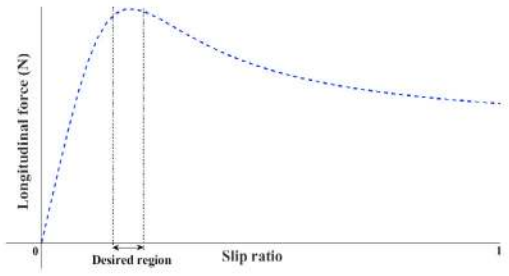

Fig. 2. Longitudinal force Vs Slip ratio

methodologies were proposed to regulate the wheel slip ratio to avoid wheel lock during braking. For example, Bhandari et al. (2012) developed slip control algorithms for a conventional passenger car based on PID (Proportional-Derivative-Integral) control and sliding mode control. The results conveyed that the sliding mode control reduces the braking distance by 4 % compared with PID control. Batayneh et al. (2018) reported that a fuzzy controller reduced the wheel slip tracking error on various road surfaces compared to the PID controller for conventional passenger car during braking. Kumar and Subramanian (2016) developed a co-operative braking control for a rear-driven electric vehicle. Savitski et al. (2016) proved experimentally that the continuous ABS control strategy reduced braking distance by 20 % compared with rule-based control strategy for an electric car.

From literature, it was observed that most of the WSR methods exist for conventional passenger car. Their suitability needs to be investigated for electrified vehicles, given the presence of regenerative braking response. Further, this study was motivated by the challenges involved in designing active braking systems for HCRVs compared to passenger cars. They include the slow response of pneumatic brake system, high load transfer from rear to the front during braking and a significant load variation between fully laden and fully unladen of the vehicle [Trigell et al. (2017)]. Typically, most of the HCRVs are rear wheel driven vehicles. Hence, this study focused on rear wheel driven electrified HCRVs. Further, amongst electric and hybrid electric vehicle configurations, the demanded motor power for Electric Vehicles (EVs) and Series Hybrid Electric Vehicles (SHEVs) is the same (for the same gear transmission ratio, gross vehicle weight and performance specification). Hence, this analysis focused on EVs and SHEVs.

Sliding Mode Control (SMC) based brake torque regulation was demonstrated in this study to achieve the desired slip ratio during vehicle braking. An important advantage of SMC is its robustness to uncertainties and disturbances [Fan et al. (2019)]. The organization of the remaining paper is as follows. The vehicle wheel dynamic model and tire model used in this study are explained in section 2. In section 3, SMC based wheel slip ratio control algorithm is presented. The proposed co-operative braking control strategy is discussed in section 4. In section 5, experimental setup and results are discussed and concluding remarks are presented in section 6.

2. VEHICLE SYSTEM MODELS

Since the study focused on the regulation of wheel slip ratio, a vehicle's wheel dynamic model and tire model are discussed below.

2.1 Vehicle's Wheel dynamic model

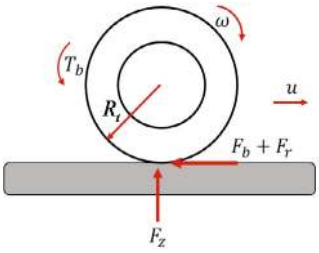

Fig. 3. Forces acting on the wheel during longitudinal motion

Figure 3 gives the forces acting on a vehicle's wheel during straight line braking, where F_b is the braking force, F_r is the rolling resistance force, F_z is the normal load acting on the wheel and T_b is the braking torque. Considering Fig. 3, wheel dynamic model can be represented as

$$I\dot{\omega}(t) = T_b(t) - (F_b(t) + F_r)\, R_t, \tag{2}$$

where I is the wheel inertia. From (1) and (2), the derivative of wheel slip ratio can be represented as

$$\dot{\lambda}(t) = \frac{R_t\omega(t)\dot{u}(t)}{u^2(t)} - \frac{R_t}{u(t)I}\left(T_b(t) - R_tF_b(t) - R_tF_r\right). \tag{3}$$

2.2 Tire model

Pacejka's Magic Formula tire model (tire size: 315/80 R 22.5) was used in this study. Figure 4 shows the longitudinal characteristic curve of the truck tire considered [IPG Automotive GmbH (2017)]. From Fig. 4, it can be observed

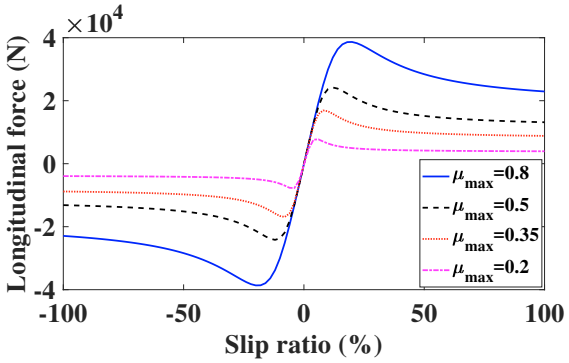

Fig. 4. Longitudinal tire characteristic curve

that the tire can generate maximum braking force for a particular range of wheel slip ratio. However, the range

of slip ratio (desired region) for the maximum braking force varies according to the road surface. An important parameter that affects braking performance of the vehicle is the maximum tire-road friction coefficient (μ_{max}) and it varies with respect to different road surfaces. In this study, 0.8, 0.5, 0.35 and 0.2 were considered as different μ_{max} values and the corresponding desired slip region was identified as (0.15-0.2), (0.1-0.15), (0.06-0.1) and (0.04-0.06) respectively from the considered truck tire data.

3. SLIDING MODE CONTROL (SMC)

Reaching law based sliding mode controller design was introduced by Huh et al. (1999). In this control method, the system consists of two modes of operation namely, reaching mode (non-sliding mode) and sliding mode. In reaching mode, the system initial state moves towards the sliding surface (defined by the user) in a finite duration. In sliding mode, the system tracks the desired trajectory (sliding surface) and thereby ensures the robustness to uncertainties and disturbances.

In this study, the sliding surface is defined as

$$S(t) = e(t) = \lambda_a(t) - \lambda_d(t), \tag{4}$$

where $\lambda_a(t)$ is the actual wheel slip ratio, $\lambda_d(t)$ is the desired wheel slip ratio, and $e(t)$ is the tracking error of wheel slip ratio during active braking. In this study, WSR was evaluated by considering Constant rate Reaching Law (CRL) and Power Rate Exponential Reaching Law (PRERL) [Devika and Thomas (2017)].

In CRL, the desired control input was obtained by

$$\dot{S}(t) = -K_{CRL} sign\left(S(t)\right), \tag{5}$$

where K_{CRL} is the controller gain. Now, considering (3) as the actual wheel slip ratio rate, from (3)-(5), the desired braking torque to achieve desired slip ratio is given by

$$\begin{aligned} T_{b,CRL}(t) = R_t\left(F_b(t) + F_r\right) + \frac{I\omega(t)\dot{u}(t)}{u(t)} \\ - \frac{u(t)I\dot{\lambda}_d(t)}{R_t} + \frac{u(t)IK_{CRL} sign\left(S(t)\right)}{R_t}. \end{aligned} \tag{6}$$

In PRERL, the desired brake torque was obtained by

$$\dot{S}(t) = \frac{-K_{PRL} \mid S(t) \mid^{\beta} sign(S(t))}{\delta_o + (1-\delta_o)e^{-\alpha|S(t)|^p}}, \tag{7}$$

where K_{PRL} is the controller gain, β, α, δ_0 and p are the controller parameters. Considering (3), (4) and (7), the desired braking torque to achieve desired slip ratio through PRERL is given by

$$\begin{aligned} T_{b,PRL}(t) = R_t\left(F_b(t) + F_r\right) + \frac{I\omega(t)\dot{u}(t)}{u(t)} - \frac{u(t)I\dot{\lambda}_d(t)}{R_t} \\ + \frac{u(t)I)}{R_t}\frac{K_{PRL} \mid S(t) \mid^{\beta} sign(S(t))}{\delta_o + (1-\delta_o)e^{-\alpha|S(t)|^p}}. \end{aligned} \tag{8}$$

Since the desired slip ratio is constant for a particular road surface, $\dot{\lambda}_d(t)$ is considered as zero. Now, the desired braking torque (6) and (8) can be written as

$$T_b(t) = T_{b,cont} + T_{b,discont}, \tag{9}$$

where $T_{b,cont}$ and $T_{b,discont}$ are continuous braking torque and discontinuous braking torque respectively. In both CRL and PRERL based SMC, the continuous braking torque input is given by

$$T_{b,cont} = R_t\left(F_b(t) + F_r\right) + \frac{I\omega(t)\dot{u}(t)}{u(t)}. \tag{10}$$

The discontinuous braking torque of SMC with CRL and PRERL respectively are

$$T_{b,discont,CRL} = \frac{u(t)IK_{CRL} sign\left(S(t)\right)}{R_t}, \tag{11}$$

and

$$T_{b,discont,PRL} = \frac{u(t)I)}{R_t}\frac{K_{PRL} \mid S(t) \mid^{\beta} sign(S(t))}{\delta_o + (1-\delta_o)e^{-\alpha|S(t)|^p}}. \tag{12}$$

Here, the discontinuous braking torque ensures that the system state reaches the sliding surface, whereas the continuous braking torque is responsible for tracking the desired sliding surface. The sharing of desired braking torque between regenerative braking and friction braking is discussed below.

4. PROPOSED CO-OPERATIVE BRAKING CONTROL STRATEGY

The electrified vehicle brake system consists of both friction brakes and regenerative brakes. The sharing of brake force between regenerative braking and friction braking is called co-operative braking. Since regenerative braking is applied only on driven wheels, the total brake force on driven wheels is shared by regenerative braking and friction braking, whereas non-driven wheels are always subjected to friction braking only.

The ratio at which the total brake force is distributed between the front and rear wheels is called Brake Force Distribution (BFD) ratio. Most of the road vehicles follow a linear BFD between the front and rear wheels. Assuming symmetric load distribution between right and left wheels, the linear BFD ratio was obtained by taking into account dynamic load transfer during braking and rolling resistance force. Typically, in linear BFD, a fixed amount of regenerative braking is applied for a constant braking demand. In this study, the amount of regenerative braking applied on driven wheels is varied to maintain the desired slip ratio. The proposed co-operative braking strategy (sharing of braking force between friction braking and regenerative braking) is as follows: In order to get desired wheel slip ratio, the continuous control input and discontinuous control input are provided by friction braking and regenerative braking respectively as explained in Fig. 5. Here, $\lambda_{f,d}$ and $\lambda_{f,a}$ indicate the desired and actual slip ratio of the front wheels respectively. $\lambda_{r,d}$ and $\lambda_{r,a}$ indicate the desired and actual slip ratio of the rear wheels respectively. $T_{bf_{fric}}$, $T_{br_{fric}}$, $T_{br_{reg}}$ indicate the front wheels friction torque, rear wheels friction torque and rear wheels regenerative torque respectively. Moreover, the process followed to obtain the driver's brake demand and the linear BFD ratio is explained in [Subramaniyam and Subramanian (2019b)].

The reasons for regulating discontinuous torque through regenerative braking are as follows: (i) Regenerative braking torque alone cannot deliver sufficient torque to get

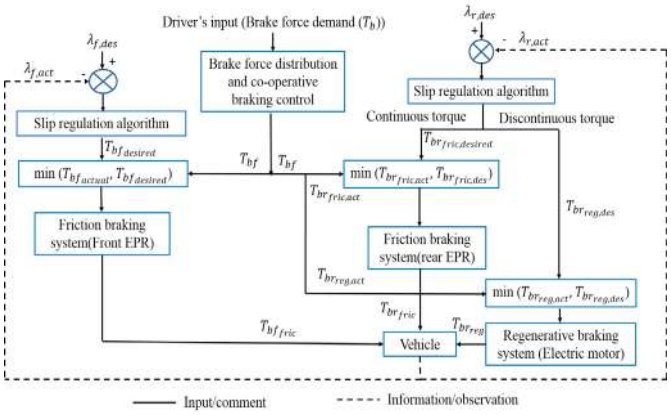

Fig. 5. Proposed co-operative braking control

adequate deceleration during braking. That is, during full braking (heavy braking), the required braking torque is much larger than the regenerative braking torque. (ii) The pneumatic braking has significant time delay (around 0.05 s) [Limpert (1999)] compared to regenerative braking. The larger time delay of the pneumatic brake system limits its bandwidth [Bu and Tan (2007)], thereby affecting the braking performance of the HCRV during ABS application. (iii) Regenerative brake system time constant (in the range of one-hundredth of a second) is very much less than the pneumatic brake system (around 0.6 s) [Crolla and Cao (2012)], [Limpert (1999)].

Further, the regenerative braking is withdrawn from driven wheels when the longitudinal vehicle speed (u) goes below the threshold speed (longitudinal vehicle speed corresponds to base speed of the motor (u_{th})) and if the battery State of Charge (SOC) reaches its higher threshold level. The regenerative braking is not recommended below u_{th} due to low energy regeneration efficiency. If the battery SOC reaches its higher threshold level then it is not possible to store the regenerated electrical energy in the battery. When the regenerative braking is not applied on the driven wheels during braking, the desired brake force is attained through friction braking only.

5. EXPERIMENTAL RESULTS AND DISCUSSION

5.1 Hardware-in-Loop Experimental setup and Realization of Regenerative braking

A 4x2 truck brake system hardware experimental setup was considered in this study (Fig. 6). An Electro-pneumatic Regulator (EPR) was used to activate the S-cam foundation brake system. The EPR input voltage regulates the pressure inside the brake chamber and this pressure was transformed to brake torque. The pressure sensor was mounted near the brake chamber to measure the brake chamber pressure. Further, the experimental setup consists of a driving module console. A load cell was mounted along with the brake pedal to measure the driver's brake pedal force. For a given brake chamber pressure, the brake torque (T_b) is calculated as

$$T_b(t) = \frac{(P_{bp}(t) - P_c)\,\eta_b A_{bc} D_{bd} L_{sa} B_f}{2R_s}, \qquad (13)$$

where P_{bp} and P_c indicates the brake chamber pressure and contact pressure respectively, η_b indicates the pneumatic brake system efficiency, A_{bc} indicates the area of the brake chamber, D_{bd} indicates the diameter of the brake drum, L_{sa} indicates the slack adjuster length, B_f indicates the brake factor and R_s indicates the S-cam radius.

Since motor is not available as hardware in the HiL platform, it have been simulated through appropriate mathematical model and integrated with the friction brake system components and the TruckMaker® vehicle simulation software through the real-time rapid prototyping hardware. A three-phase induction motor was considered in this study to derive the appropriate dynamic motor model and the regenerative braking torque was regulated using the same [Subramaniyam and Subramanian (2019a)].

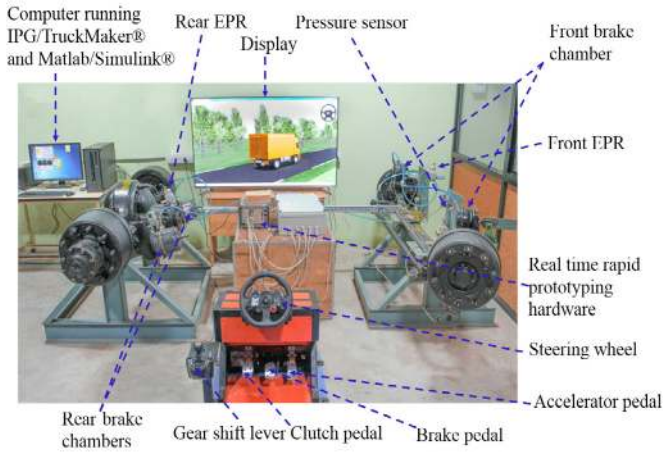

Fig. 6. Hardware-in-Loop brake system experimental setup

5.2 Experimental Results and Discussion

The maximum energy regeneration and thereby change in the battery SOC during one full (hard) braking process is very small. Hence, in this study, it was assumed that during braking the battery SOC does not reach its higher threshold value. In addition to this, it was assumed that the battery SOC is not near to its higher threshold value during initiation of braking. With this assumption, in this study, it was considered that the extent of regenerative braking was decided by only vehicle longitudinal speed.

To implement the proposed co-operative strategy with SMC in HiL brake system experimental setup, parameters such as vehicle's longitudinal speed, longitudinal acceleration and actual wheel angular speed are required. These parameters were assumed as readily available and were considered from TruckMaker® commercial vehicle software. Further, it was assumed that the vehicle was running straight on the symmetric road surface (right and left wheels of the vehicle running on road of same μ_{max}). The vehicle parameters considered in the study are shown in Table 1.

Initially, SMC with CRL and PRERL were compared by considering a fully unladen vehicle on the road surface which has μ_{max} of 0.8 with the braking speed of 20 m/s. Since a rear wheel driven electrified HCRV was considered in this study, during braking, the total brake force on rear

Table 1. Vehicle parameters

Parameter	Laden	Unladen
Vehicle mass	16200 kg	4700 kg
Wheel base	5.4 m	5.4 m
Height of Centre Gravity (CG)	1.3 m	1 m
The distance between the front axle and CG	3.4 m	2.7 m

wheels was shared by regenerative braking and friction braking, whereas the front wheels were always subjected to friction braking only. In case of conventional braking, both front and rear wheels were subjected to friction braking only. Figure 7 gives the comparison of the performance of the rear wheel slip ratio during conventional braking and co-operative braking for CRL based control input.

It can be observed that the SMC with CRL introduces chattering (oscillation) in the wheel slip ratio during braking because of the 'sign' term present in the reaching law. Further, it was noticed that the co-operative braking introduces more oscillation on slip ratio compared to conventional braking because of the high bandwidth of regenerative braking compared to conventional braking. As mentioned earlier, once the longitudinal vehicle speed reaches u_{th} during braking, the regenerative braking is withdrawn from driven wheels and the demanded brake force is applied through friction braking only. This process is called braking blend-out and the same can be observed in Fig. 7.

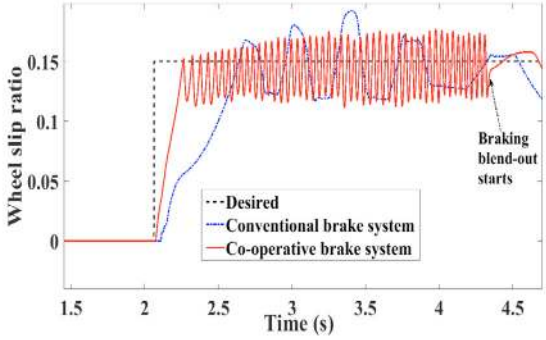

Fig. 7. Comparison of co-operative braking and conventional braking with CRL

The performance of reaching law was evaluated by calculating the Mean Absolute Percentage Error (MAPE) between the desired slip ratio and actual slip ratio. MAPE is defined as

$$MAPE = \frac{1}{N}\left(\sum_{i=1}^{N}\frac{|\lambda_d - \lambda_a|}{\lambda_d}\right)100\%, \qquad (14)$$

where N is the number of samples. For a fully unladen vehicle on $\mu_{max} = 0.8$ road, the MAPE with CRL for conventional and co-operative braking are 24.8 % and 15.22 % respectively. High tracking error was noticed with conventional baking compared to co-operative braking. This was due to high response time and lower bandwidth of conventional brake system compared to regenerative brake system.

To reduce the chattering during WSR, SMC with PRERL was introduced. Due to the presence of the exponential term in PRERL, the chattering in the slip ratio was reduced. Figure 8 shows the comparison of rear-wheel slip ratio during conventional braking and co-operative braking for PRERL based control input. Here, the MAPE was 15.43 % and 8.73 % for conventional and co-operative braking respectively. It can be observed that the SMC with PRERL minimizes the chattering effect and thereby reduces the slip ratio tracking error compared to SMC with CRL.

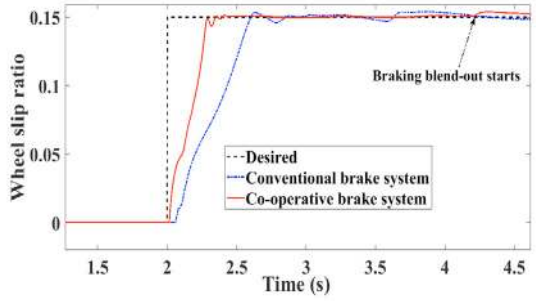

Fig. 8. Comparison of co-operative braking and conventional braking with PRERL

Further, the CRL and PRERL performance were evaluated by considering the vehicle's stopping distance. The stopping distance for SMC with CRL and PRERL were 29.94 m and 29.13 m respectively with a proposed co-operative strategy for a fully unladen vehicle on $\mu_{max} = 0.8$ road surface with an initial braking speed of 20 m/s. Here, it can be observed that the SMC with PRERL reduces the stopping distance by 2.7 % compared to SMC with CRL due the reduction of chattering in wheel slip ratio and thereby in vehicle deceleration during co-operative braking. The comparison of vehicle deceleration during braking with CRL and PRERL is shown in Fig. 9.

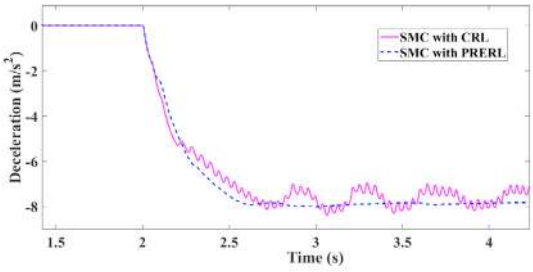

Fig. 9. Comparison of deceleration with CRL and PRERL during co-operative braking

The sensitivity analysis was carried out with respect to μ_{max} value and longitudinal vehicle speed for the proposed co-operative strategy with PRERL based control input. The minimum initial braking speed for different μ_{max} road surfaces was decided as per the Federal Motor Carrier Safety Administration (FMCSA) recommendation. In order to evaluate the performance of SMC with PRERL, a fully laden electrified HCRV was considered. During braking, the dynamic load transfer from rear to front is higher for a fully laden vehicle compared to fully unladen vehicle. The slip ratio MAPE and stopping distance for different operating conditions are shown in Table 2.

Table 2. Comparison of conventional braking and proposed co-operative braking for fully laden vehicle

Operating Condition		Slip ratio MAPE (%)		Stopping distance (m)	
μ_{max}	Longitudinal speed (m/s)	Conventional braking	Co-operative braking	Conventional braking	Co-operative braking
0.5	16.67	11.75	10.8	32.33	31.98
0.5	13.33	14.16	11.78	21.39	20.64
0.35	13.89	8.75	8.12	32.57	31.83
0.35	10	11.2	8.87	17.97	17.43
0.2	11.11	8.2	7.7	34.13	33.9
0.2	8.33	9.6	8.5	20.12	19.69

From the sensitivity analysis, the following observations are made: Both conventional and co-operative braking reduces the slip ratio MAPE as speed increases on a particular road surface. This was due to an increase of braking duration for higher initial braking speed compared to lower initial braking speed. As μ_{max} value decreases (for different road surfaces), slip ratio MAPE is reduced due to decrease of desired slip ratio and thereby demanded brake pressure or regenerative torque.

The reduction in the stopping distance with co-operative braking can be attributed to the quicker response of regenerative braking. Further, the maximum and minimum reduction in stopping distance with co-operative braking are 3.5 % and 0.6 % on $\mu_{max} = 0.5$ road surface and $\mu_{max} = 0.2$ road surface respectively. As the demanded braking torque on $\mu_{max} = 0.2$ road surface was low to begin with, no significant improvement was achieved with co-operative braking.

6. CONCLUSIONS

Reaching law based SMC was developed to regulate the wheel slip ratio of an electrified HCRV during braking by exploiting the advantages of regenerative braking. The impact of reaching law on WSR was studied by considering CRL and PRERL. The experimental results conveyed that the SMC with PRERL reduces the chattering in wheel slip ratio and thereby stopping distance compared to SMC with CRL. Further, a sensitivity analysis was carried out for different values of μ_{max} and longitudinal vehicle speed. It was observed that co-operative braking reduces the slip ratio tracking error and thereby stopping distance compared to conventional braking. The investigation of interaction between regenerative braking and friction braking on split traction road surfaces and during cornering (where the right and left wheel rotation speeds are different) will be considered as future work.

REFERENCES

Allen, K. (2010). The effectiveness of abs in heavy truck tractors and trailers. Technical report.

Batayneh, W., Jaradat, M., and Bataineh, A. (2018). Intelligent adaptive control for anti-lock braking system. In *ASME 2018 International Mechanical Engineering Congress and Exposition*, V04AT06A006–V04AT06A006. American Society of Mechanical Engineers.

Bhandari, R., Patil, S., and Singh, R.K. (2012). Surface prediction and control algorithms for anti-lock brake system. *Transportation research part C: emerging technologies*, 21(1), 181–195.

Bu, F. and Tan, H.S. (2007). Pneumatic brake control for precision stopping of heavy-duty vehicles. *IEEE Transactions on Control Systems Technology*, 15(1), 53–64.

Crolla, D.A. and Cao, D. (2012). The impact of hybrid and electric powertrains on vehicle dynamics, control systems and energy regeneration. *Vehicle system dynamics*, 50(sup1), 95–109.

Devika, K. and Thomas, S. (2017). Power rate exponential reaching law for enhanced performance of sliding mode control. *International Journal of Control, Automation and Systems*, 15(6), 2636–2645.

Fan, C., Hong, G.S., Zhao, J., Zhang, L., Zhao, J., and Sun, L. (2019). The integral sliding mode control of a pneumatic force servo for the polishing process. *Precision Engineering*, 55, 154–170.

Huh, K., Seo, C., Kim, J., and Hong, D. (1999). An experimental investigation of a cw/ca system for automobiles using hardware-in-the-loop simulations. In *Proceedings of the 1999 American Control Conference (Cat. No. 99CH36251)*, volume 1, 724–728. IEEE.

IPG Automotive GmbH (2017). IPG TruckMaker® Reference Manual Version 6.0.5.

Kumar, C.N. and Subramanian, S.C. (2016). Cooperative control of regenerative braking and friction braking for a hybrid electric vehicle. *Proceedings of the Institution of Mechanical Engineers, Part D: Journal of Automobile Engineering*, 230(1), 103–116.

Limpert, R. (1999). *Brake design and safety*. SAE.

Ministry of Road Transport & Highways, Transport Research Wing (New Delhi, India, 2017.). Road accidents in india. Technical report, Office of Ministry of Road Transport & Highways.

Savitski, D., Ivanov, V., Augsburg, K., Shyrokau, B., Wragge-Morley, R., Pütz, T., and Barber, P. (2016). The new paradigm of an anti-lock braking system for a full electric vehicle: experimental investigation and benchmarking. *Proceedings of the Institution of Mechanical Engineers, Part D: Journal of Automobile Engineering*, 230(10), 1364–1377.

Subramaniyam, K.V. and Subramanian, S.C. (2019a). Analysis of cornering response and stability of electrified heavy commercial road vehicles with regenerative braking. *Proceedings of the Institution of Mechanical Engineers, Part D: Journal of Automobile Engineering*, 0954407019890157.

Subramaniyam, K.V. and Subramanian, S.C. (2019b). Impact of regenerative braking torque blend-out characteristics on electrified heavy road vehicle braking performance. *Vehicle System Dynamics*, 1–26.

Trigell, A.S., Rothhämel, M., Pauwelussen, J., and Kural, K. (2017). Advanced vehicle dynamics of heavy trucks with the perspective of road safety. *Vehicle system dynamics*, 55(10), 1572–1617.

World Health Organization (2018). Global status report on road safety 2018. Technical report.